Analysis of the vehicle brake judder problem by employing a simplified source–path–receiver model

C Duan and **R Singh***
Acoustics and Dynamics Laboratory, Department of Mechanical Engineering, The Ohio State University, Columbus, Ohio, USA

The manuscript was received on 5 May 2010 and was accepted after revision for publication on 17 September 2010.

DOI: 10.1177/09544070JAUTO1629

Abstract: An analytical formulation of the brake judder problem caused by disc thickness variation is described by using a simplified source–path–receiver model. Eigenvalue analysis is first conducted to determine the transfer mechanism from the brake source to the steering-wheel receiver. Calculations show that the peak vibration levels of the steering wheel are seen when the rotational frequency of the tyre coincides with the resonant frequency of the transfer path; in this case, only the first-order disc thickness variation is considered. The effects of two key parameters, associated with the source and the path respectively, are analytically and computationally studied. Analysis suggests that the lower pad stiffness and/or the higher bushing stiffness should effectively reduce the vibration levels. Finally, a new vibration control concept is proposed that modulates the actuation pressure; it is based on an approximate solution for the angular displacement of the disc in the model developed here. Preliminary work indicates that this concept could be very effective in reducing the receiver vibration level without sacrificing the brake performance.

Keywords: brake judder, frictional system analysis, transient vibration

1 INTRODUCTION

Vehicle brake judder is a transient vibration problem that occurs during high-speed braking events. It is mainly caused by brake disc thickness variation (DTV), which arises owing to the uneven finish of the brake disc resulting from the manufacturing problem (cold judder), the uneven wear due to a 'hard' pad or harsh operating environment, or the heat-induced thickness variation (hot judder) [**1**–**11**]. In the presence of frictional contacts and pad stiffness, the DTV essentially induces a time-varying torque [**1**]. The brake torque variation (BTV) is then transmitted through chassis elements to the steering wheel in the form of low-frequency oscillations in the tangential direction; it is sometimes called steering-wheel nibble. Given customer satisfaction issues and costly warranty repairs, brake judder has attracted some attention from both industry and academia [**1**–**12**]. Jacobsson [**1**, **2**] has summarized pre-2003 literature well and has discussed pertinent issues.

Previous literature could be grouped into two categories. For instance, one group of researchers has focused on the source that consists of the brake rotor and pad subsystem [**1**–**6**]. Jacobsson [**2**] has developed amplitude functions to estimate the peak amplitude of the source by using a caliper–rotor type of model. Cho *et al.* [**5**] studied the hot spots caused by brake judder using experiments and finite element analysis. Kang and Choi [**6**] have calculated the BTV due to the DTV by utilizing a model of the brake dynamometer. The second group of researchers has examined the transfer path issues, from the BTV to the steering-wheel vibration [**7**–**11**] by using computational models and/or experimental work. For example, Gassmann and Engel [**7**] investigated the transfer mechanism by using an experimental method and concluded that it is necessary to address the system problem including the brakes, suspension, and steering wheel. Meyer [**10**] found a strong correlation between wishbone resonance and steer-

**Corresponding author: Acoustics and Dynamics Laboratory, Department of Mechanical Engineering, The Ohio State University, Columbus, OH 43210, USA.*
email: singh.3@osu.edu

ing-wheel vibration. By assuming out-of-phase brake torque excitation on the right and left wheels, Meyer [**10**] studied the effect of the bushing stiffness.

Although some progress has been made over the last decade, an analytical system-level model is yet to be developed. Multi-body dynamics models [**10**, **11**] could yield reasonable results but they could be very complex and vehicle specific. For example, Meyer [**10**] employed a 56-degrees-of-freedom model to study the judder issue. Therefore, this article will attempt to develop an analytical model to understand the system dynamics conceptually. The analytical formulation focuses on the general judder problem and does not intend to address any brake caliper design or vehicle-specific issues. Possible solutions that could mitigate judder are proposed and some qualitative comparisons with previous work will be made.

2 PROBLEM FORMULATION

A conceptual source–path–receiver model is proposed, as shown in Fig. 1. Here, the source regime includes the pad and brake disc inertia frictional contact and the actuation pressure $P(t)$. The structural path is composed of a lumped suspension inertia element and a linear torsional spring that represents the steering tie-rod and rack–pinion subsystem. The steering wheel is the receiver and is represented by a rotational moment of inertia. The primary excitation is assumed to be from the brake DTV $u(t)$ that could be caused by manufacturing, wear, or heat-induced distortions. This motion input induces a dynamic torque $T(t)$, which would excite the suspension system in the form of fore–aft and/or rotational oscillations, and ultimately the vibration is transmitted to the driver, in the form of torsional oscillations at the steering wheel [**8**, **10**].

In Fig. 1, I_d represents the equivalent vehicle moment of inertia as perceived by the brake disc. It is estimated using the equivalent kinetic energy approach $0.5 m_\mathrm{vehicle} V_0^2 = 0.5 I_\mathrm{d} \Omega_\mathrm{d}^2$, where V_0 is the initial vehicle speed, Ω_d is the corresponding disc speed, and m_vehicle is the mass of the vehicle. This leads to $m_\mathrm{vehicle} V_0^2 = I_\mathrm{d} \left(V_0 / r_\mathrm{tyre}\right)^2$, or $m_\mathrm{vehicle} r_\mathrm{tyre}^2 = I_\mathrm{d}$, where r_tyre is the tyre radius. Note that, when a single front wheel is considered, accounting for front–rear brake proportioning, the kinetic energy used to estimate I_d should be a portion of the total vehicle energy. In addition, I_s and I_t represent the equivalent suspension and steering system moments of inertia respectively. Consider the most common suspension (Macpherson front), where an A-type control arm links the suspension and vehicle subframe, as shown in Fig. 2. $T(t)$ excites the suspension in the fore–aft or torsional direction, and oscillations in either direction would cause a twist in the rubber bushing that mainly constrains the control arm [**7**–**10**]. Therefore, an equivalent non-linear torsional stiffness K_b of bushing is included. The brake pad–rotor contact regime is assumed to be linear and given by the translational damping element K_p and the viscous pad damping element C_p. The dry-friction regime is also considered. The actuation pressure $P(t)$ is assumed to vary (or even to modulate) with time. Finally, K_t and C_t are assumed to be linear torsional spring and viscous damping terms respectively which represent the steering system.

The system model has two non-linear interactions: one is the friction non-linearity at the pad contact and the other is the stiffness non-linearity associated with the bushings. The governing equations are written by assuming a sinusoidal DTV $u(t)$ in the amplitude D according to

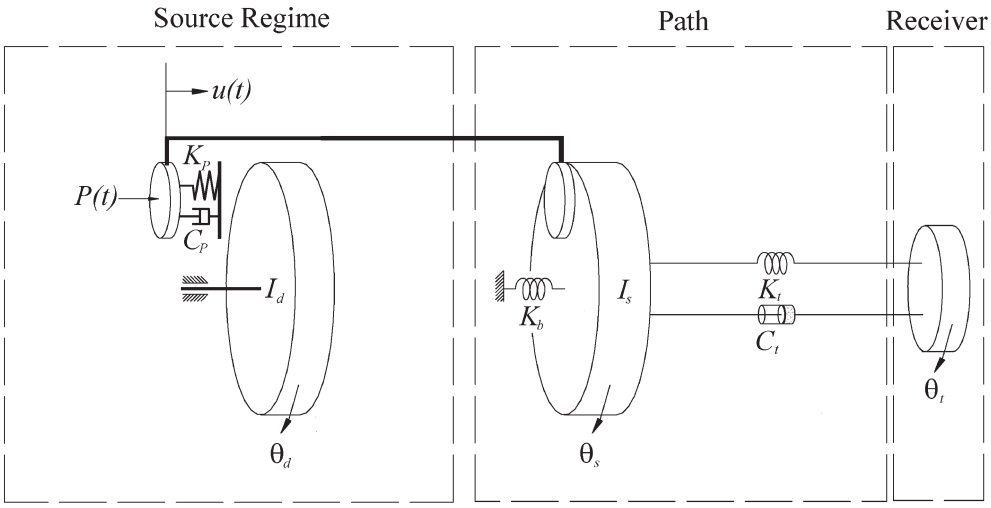

Fig. 1 A simplified source–path–receiver model for brake judder analysis

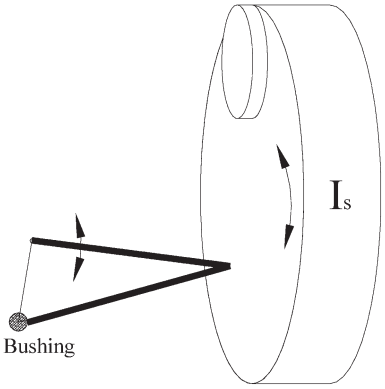

Fig. 2 Kinematics of the suspension, control arm, and rubber bushing

$$I_d\ddot{\theta}_d = T(t) = -2\mu R_{eff}\left[P(t)A + C_p\dot{u}(t) + K_p u(t)\right] \quad (1)$$

$$u(t) = D\cos[\theta_d(t)] \quad (2)$$

$$I_s\ddot{\theta}_s + C_t\left(\dot{\theta}_s - \dot{\theta}_t\right) + K_t\left(\dot{\theta}_s - \dot{\theta}_t\right) + K_b\dot{\theta}_s = 2\mu R_{eff}\left[P(t)A + C_p\dot{u}(t) + K_p u(t)\right] \quad (3)$$

$$I_t\ddot{\theta}_t - C_t\left(\dot{\theta}_s - \dot{\theta}_t\right) - K_t(\theta_s - \theta_t) = 0 \quad (4)$$

Here, θ_d, θ_s, and θ_t are the angular displacements of the brake disc, suspension, and steering system respectively. Additionally, μ is the friction coefficient, R_{eff} is the effective radius of contact area, and A is the effective pressure actuation area. Note that it is assumed that the same actuation pressures and pad stiffnesses are applied on the two sides of the brake disc. If not, equation (1) should be modified.

In practice, the suspension and steering subsystems would be difficult to re-engineer to attenuate the brake judder problem; their parameters are thus not varied during the course of this study. Consequently, the chief objective of this study is to investigate the transfer mechanism from the source to the receiver and to study the effects of K_p and K_b on $T(t)$ and the steering-wheel vibration $\theta_t(t)$. Following an approximate analytical solution of $\theta_d(t)$, a novel strategy that modulates $P(t)$ is proposed to counteract theoretically the vibration caused by $T(t)$.

3 TYPICAL BRAKE JUDDER RESPONSE

The nominal values of the parameters and excitation levels used to simulate the system of Fig. 1 are listed in Table 1. A 195/55R15 size tyre is considered and its radius is assumed to have a 5 per cent compression under a typical vehicle load. For this reason, its effective dynamic radius can be calculated as $r_{tyre} = 0.2924$ m. Since the transient (time domain) response is of interest, the initial vehicle speed V_0 is set at 150 km/h; this corresponds to an equivalent initial rotational speed $\dot{\theta}_d(0)$ of 142.5 rad/s. Without loss of generality, other initial conditions are as follows: $\theta_d(0) = 0$, $\theta_s(0) = 2\mu R_{eff}K_pD/K_b$, $\dot{\theta}_s(0) = 0$, $\theta_t(0) = 0$, and $\dot{\theta}_t(0) = 0$. A constant-pressure profile $P(t) = P_{max}$, following a quick ramp-up, is considered in preliminary calculations.

Equations (1) to (4) are numerically solved using the Runge–Kutta method. Given different orders of stiffness values (in Table 1), a variable-order (ode15s) scheme in MATLAB is employed as it is designed to solve stiff differential equations. Given the initial conditions, the calculated responses are shown in Figs 3 and 4, where t_s is the time taken to bring the vehicle to a stop ($V = 0$). As seen in Fig. 3, the vehicle decelerates almost linearly (beyond $t = t_c$) in response to a constant brake pressure, following a short quadratic decline corresponding to the pressure ramp-up stage (from $t = 0$ to t_c). Observe that the

Table 1 Nominal values of parameters and excitation used for the system of Fig. 1

Parameter	Value	Note
μ	0.4	Dry friction coefficient
R_{eff}	0.18 m	—
A	0.0084 m^2	With assumed pad dimensions (127 mm × 66 mm)
D	40×10^{-6} m	Typically 30–50 μm
I_d	120 kg m^2	Reflected vehicle moment of inertia on brake disc
I_s	1.5 kg m^2	—
I_t	0.2 kg m^2	—
C_p	1×10^6 N s/m	—
C_t	2N.m.s/rad	—
K_p	9.0×10^7 N/m	Value for a specific pressure
K_b	1.0×10^5 N m/rad	Linearized stiffness when the operating point is around the origin
K_t	1.8×10^3 N m/rad	—
P_{max}	20×10^5 Pa	—

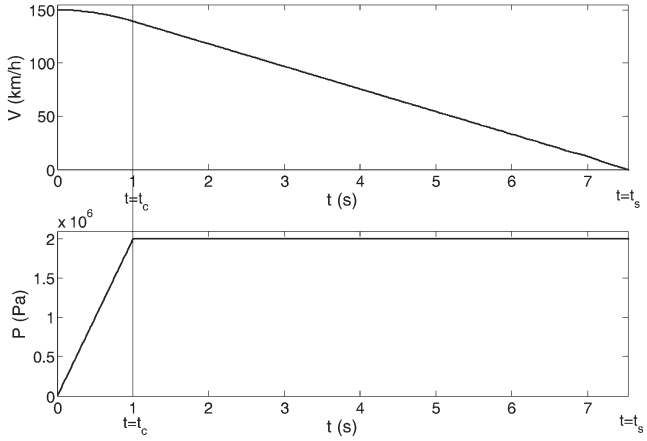

Fig. 3 Vehicle deceleration $V(t)$ and pressure $P(t)$ profiles

wheel response θ_t depends on the vehicle speed V, as shown in Fig. 4(a). A resonant peak occurs at 93.5 km/h; it is equivalent to a tyre rotational frequency $\dot{\theta}_{\text{tyre}}$ of 14.1 Hz. It is explained by an eigenvalue analysis of the linearized source–path–receiver system. Define

$$(\mathbf{K}-\omega^2\mathbf{I})\boldsymbol{\Theta}=\mathbf{0} \tag{5}$$

where

$$\mathbf{I}=\begin{bmatrix} I_s & 0 \\ 0 & I_t \end{bmatrix} \tag{6}$$

$$\mathbf{K}=\begin{bmatrix} K_b+K_t & -K_t \\ -K_t & K_t \end{bmatrix} \tag{7}$$

Two natural frequencies and their eigenvectors are obtained, given the nominal parameters of Table 1: $\omega_1 = 14.9\,\text{Hz}$ and $\omega_2 = 41.5\,\text{Hz}$; $\boldsymbol{\Theta}_1 = [0.02 \quad 1]^T$ and $\boldsymbol{\Theta}_2 = [1 \quad -0.15]^T$. By comparing the vibration amplitudes of θ_t in Fig. 4(a) and θ_s in Fig. 4(b), it is seen that the system is excited at ω_1; this is also validated by Fig. 4(c) which shows the frequency domain components of θ_t. Indeed, previous researchers have reported a similar resonant frequency of the steering-wheel vibration [**7**, **12**]. The present results are also similar to those observed by Meyer [**10**] who obtained speed-dependent wheel responses using experimental and computational methods.

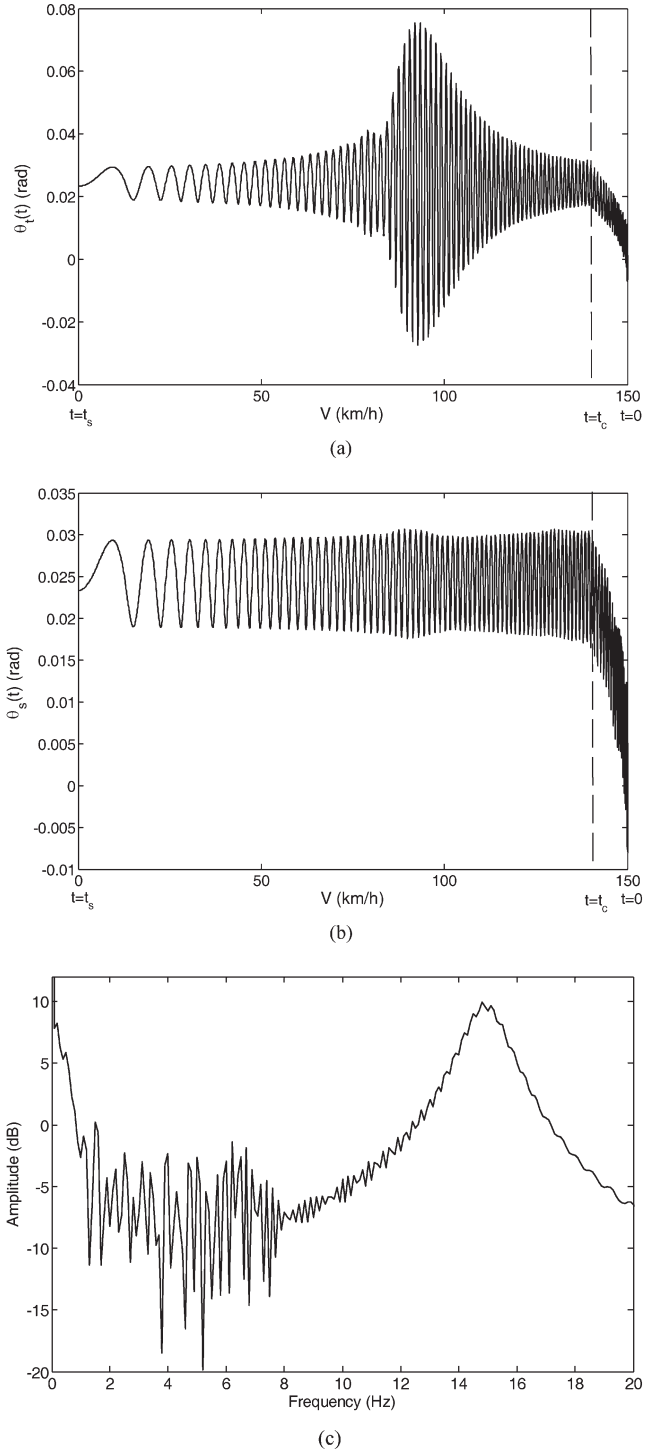

Fig. 4 Typical angular displacements under the judder condition: (a) steering-wheel vibration $\theta_t(t)$; (b) suspension system vibration $\theta_s(t)$; (c) fast Fourier transform of $\theta_t(t)$

4 EFFECTS OF THE NON-LINEAR PAD STIFFNESS

The brake pad–rotor contact regime should be quantified by a non-linear stiffness function under compression. For example, Kang and Choi [**6**] suggested typical brake pad stiffness values over a range of loads. A second-order polynomial was used to curve-fit the non-linear stiffness–pressure relationship

successfully. Similarly, a second-order $K_p(P)$ expression given by

$$K_p(P) = a_0 + a_1 P + a_2 P^2 \tag{8}$$

is employed in this study, with $a_0 = -2\times10^7$, $a_1 = 80$, and $a_2 = -1.25\times10^{-5}$. During a specific braking event, a constant pressure P_{max} is applied following a ramp-up, as shown in Fig. 3. A closer inspection of equation (1) finds that a reduction in K_p (or a softer pad) could lower $T(t)$ since its alternating component is given by $2\mu R_{eff}\left[C_p\dot{u}(t) + K_p u(t)\right]$. Further, the torque excitation to the suspension–steering subsystem could be reduced as seen from equation (3) and consequently $\theta_t(t)$ would also be attenuated. Assuming a linearized (constant) bushing stiffness value, numerical results for three actuation pressures are presented in Fig. 5. Clearly, a reduction in P_{max} decreases $\theta_t(t)$. This numerical result is in good agreement with the above postulation. Indeed, a reduction in K_p is comparable with lower DTV values, as seen by equation (1). This finding is consistent with the brake pad–rotor investigation by Kang and Choi [**6**].

5 EFFECT OF THE BUSHING STIFFNESS

The model shown in Fig. 1 suggests that a rigid bushing should theoretically isolate the steering subsystem from the brake subsystem. Figure 6 shows results for several linearized K_b values. Observe that a higher value of K_b effectively reduces the steering-wheel vibration. The mean value of $\theta_t(t)$ also changes together with the mean of θ_s, which can be approximated by $2\mu R_{eff}P_{max}A/K_b$ from equation (3) after the initial ramp-up of $P(t)$. Further, as defined in equations (5) to (7), a change in K_b will vary the system's natural frequencies only marginally, and these frequencies are still dominated by K_t and I_t. For example, the $0.5K_b$ value will only downshift the first mode from 14.9 Hz to 14.8 Hz, and the $2K_b$ value upshifts the mode from 14.9 Hz to only 15.0 Hz.

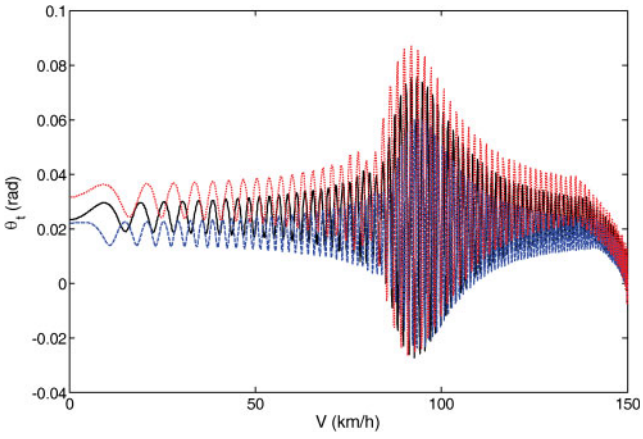

Fig. 5 Effect of the actuation-pressure-dependent pad stiffness on the steering-wheel vibration: ——, $P_{max} = 2\times10^6$ Pa; -----, $P_{max} = 1.5\times10^6$ Pa; •••••, $P_{max} = 2.5\times10^6$ Pa

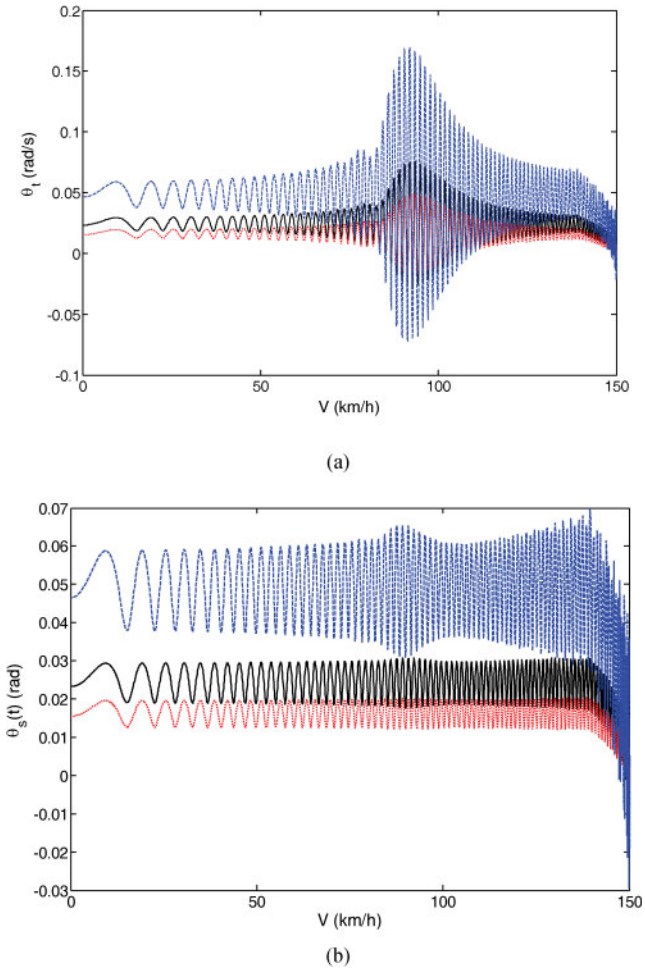

Fig. 6 Effect of the rubber bushing stiffness K_b on the (a) the steering-wheel vibration and (b) the suspension system vibration: ——, $K_b = 1.0\times10^5$ N m/rad; -----, $K_b = 0.5\times10^5$ N m/rad; •••••, $K_b = 1.5\times10^5$ N m/rad

Further, the non-linearity of the rubber bushing has been mentioned by a few researchers [**7**, **9**]. Accordingly, the bushing is modelled with both a quadratic and a cubic non-linear torque–angular-displacement relationship according to

$$T_b(\theta_b) = K_{bn}\theta_s\left(1 + \alpha\theta_s + \beta\theta_s^2\right) \tag{9}$$

where K_{bn} is the linearized stiffness when the mean displacement is zero, and α and β are coefficients of

the non-linear terms. As shown in Fig. 7, a hardening-type spring is observed by assuming that $\alpha = 0.3$ and $\beta = 5$. Results obtained from both non-linear and linearized bushing stiffness models are shown in Fig. 8. No differences between the two results are seen in either θ_t or θ_s. This is attributed to a small variation in θ_s, especially when $\theta_s(t)$ operates around $\theta_s = 0$. Hence the non-linear stiffness yields almost the same results as the linear model.

6 EFFECT OF THE ACTUATOR PRESSURE MODULATION

The previous sections suggests that the receiver vibration could be attenuated using source (K_p) and/or path (K_b) parameters. With the advent of modern electronic control systems, such as anti-lock braking or an electronic stability control system, a direct reduction in excitation at the source is possible. For example, Wu and Shih [**13**] numerically and experimentally controlled the brake hydraulic pressure at higher frequencies. This idea was inspired by previous work of the present authors [**14**, **15**] on modulated dry-friction path control.

To reduce the receiver vibration by modulating $P(t)$, an approximate analytical solution of $\theta_d(t)$ is first developed. As shown in Fig. 3, the vehicle exhibits minimal speed fluctuations until it is brought to a complete stop. From equation (1), on the assumption that $u(t) = 0$, the rotor disc acceleration is approximated by

$$\ddot{\theta}_d(t) \approx -2BP(t) \tag{10}$$

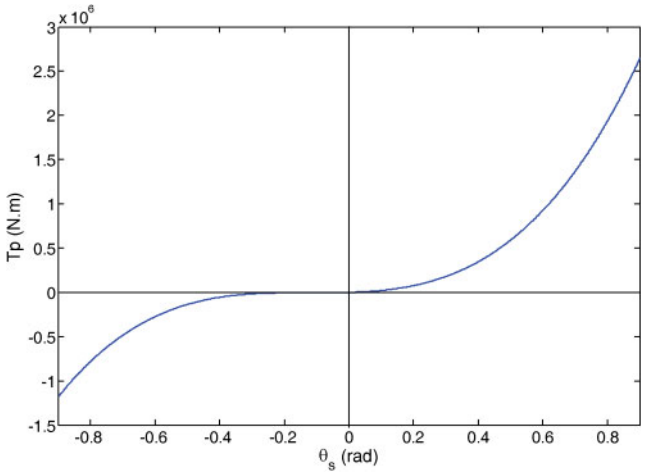

Fig. 7 Non-linear characteristics of the rubber bushing stiffness

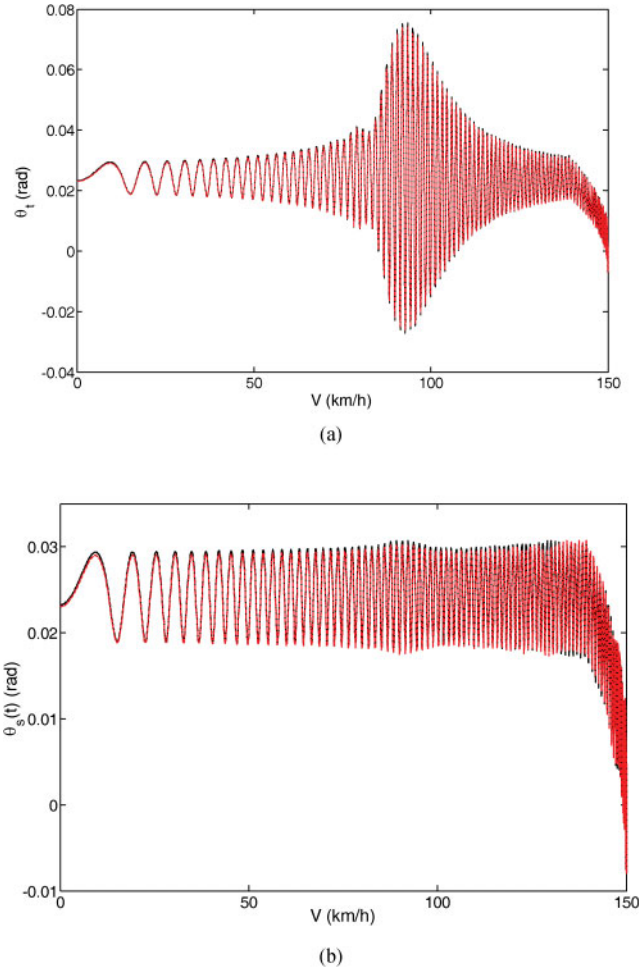

Fig. 8 Effect of the rubber bushing non-linearity on the (a) the steering-wheel vibration $\theta_t(t)$ and (b) the suspension system vibration $\theta_s(t)$: ——, linearized model; •••••, non-linear model

where $B = \mu R_{eff} A / I_d$. For the hydraulic pressure profile in Fig. 3(b), the $\dot{\theta}_d(t)$ expression is derived in two stages.

1. When $0 \leqslant t \leqslant t_c$

$$\begin{aligned}\dot{\theta}_d(t) &\approx \int -2BP(t)\,dt \\ &= \int -2B\frac{P_{max}}{t_c}t\,dt \\ &= -B\frac{P_{max}}{t_c}t^2 + c_1 \end{aligned} \tag{11}$$

Here, c_1 is a constant of integration. Since the initial condition $\dot{\theta}_d(0) = \Omega_{wheel}$, c_1 is found. Now

$$\dot{\theta}_d(t) \approx -B\frac{P_{max}}{t_c}t^2 + \Omega_{wheel} \tag{12}$$

Further

$$\theta_d(t) \approx \int \left(-B\frac{P_{max}}{t_c}t^2 + \Omega_{wheel} \right) dt$$
$$= -B\frac{P_{max}}{3t_c}t^3 + \Omega_{wheel}t + c_2 \quad (13)$$

Since $\theta_d(t) = 0$

$$\theta_d(t) \approx \int \left(-B\frac{P_{max}}{t_c}t^2 + \Omega_{wheel} \right) dt$$
$$= -B\frac{P_{max}}{3t_c}t^3 + \Omega_{wheel}t \quad (14)$$

2. When $t_c < t \leqslant t_s$

$$\dot{\theta}_d(t) \approx \int -2BP(t)\, dt$$
$$= -2BP_{max}t + c_3 \quad (15)$$

Application of the initial condition $\dot{\theta}_d(t_c) = -BP_{max}t_c + \Omega_{wheel}$ gives

$$\dot{\theta}_d(t) \approx -2BP_{max}t + (BP_{max}t_c + \Omega_{wheel}) \quad (16)$$

Further

$$\theta_d(t) \approx \int [-2BP_{max}t + (BP_{max}t_c + \Omega_{wheel})]\, dt \quad (17)$$

Application of the initial condition at $t = t_c$ yields again $\theta_d(t_c) = -\frac{1}{3}BP_{max}t_c^2 + \Omega_{wheel}t_c$. Finally, it is found that

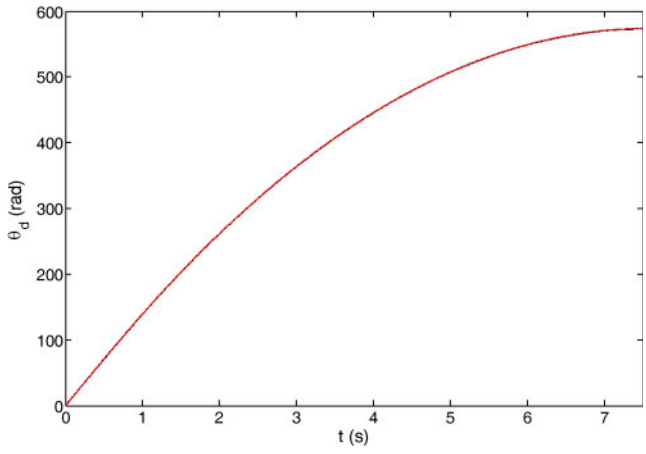

Fig. 9 Comparison of the numerical and analytical solutions of $\theta_d(t)$: ——, numerical integration; •••••, analytical solution

$$\theta_d(t) \approx -BP_{max}t^2 + (BP_{max}t_c + \Omega_{wheel})t - \frac{1}{3}BP_{max}t_c^2 \quad (18)$$

Figure 9 compares the approximate analytical solution with numerical integration. It is evident that the analytical solution is very accurate.

Given the analytical solution, a modulated pressure concept is now applied to suppress the judder-induced vibration. Specifically, an out-of-phase oscillatory component could be added to counteract the effect of $K_p u(t) = K_p D \cos[\theta_d(t)]$. For example, a modulated pressure signal could possibly be designed as

$$P(t) = \begin{cases} \frac{P_{max}}{t_c}t - \varepsilon P_{max}\cos[\theta_d(t)], & 0 \leqslant t \leqslant t_c \\ P_{max} - \gamma P_{max}\cos[\theta_d(t)], & t_c < t \leqslant t_s \end{cases} \quad (19)$$

where ε and γ represent coefficients in two actuation regimes. Since the main interest is when $t > t_c$, an arbitrarily small number can be assigned to ε. To maximize the counter-action beyond t_c, γ is determined from

$$\gamma = \frac{K_p D}{P_{max}A} \quad (20)$$

Figure 10 shows the effect of modulated $P(t)$ on θ_t. It is seen that the receiver vibration has been significantly reduced. For example, the peak-to-peak response (at 94 km/h) is reduced by 52 per cent. Interestingly, the modulated pressure does not introduce any oscillations to the vehicle speed during deceleration. This indicates that the braking performance has not been adversely impacted.

7 CONCLUSION

In this study, the brake judder problem caused by DTV is analytically studied using a simplified source–path–receiver model. Three contributions emerge. First, eigenvalue analysis is carried out to examine the transfer path mechanism from the judder source (DTV) to the receiver (steering wheel). It is observed that the steering-wheel vibration peaks when the tyre rotation coincides with the path resonant frequency; only the first-order DTV is considered in the present analysis. Second, the effects of two key parameters, associated with the source and the path respectively, are studied. It is

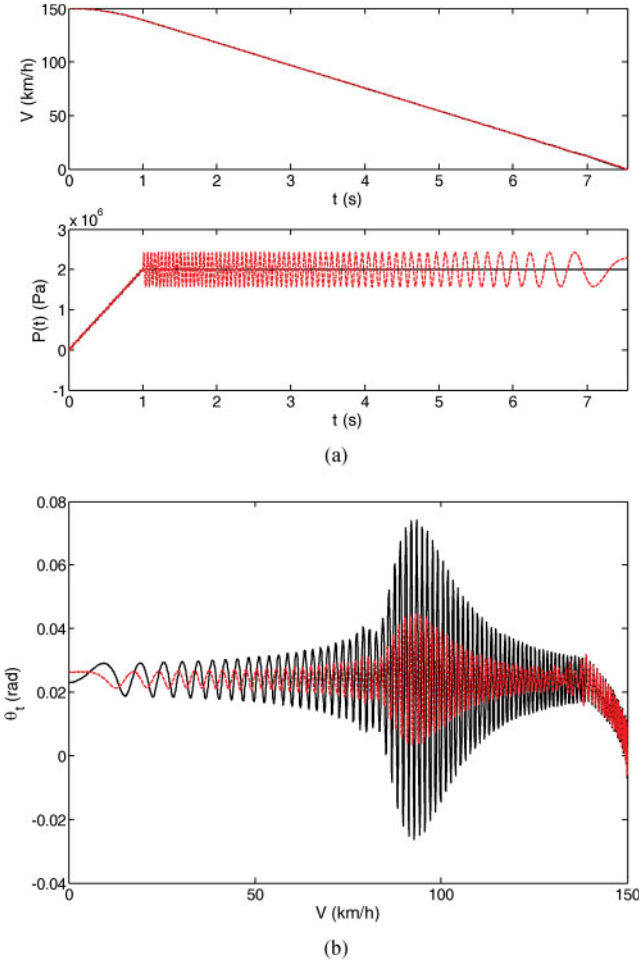

Fig. 10 Effect of the modulated pressure $P(t)$ on judder for (a) the vehicle deceleration $V(t)$ and pressure $P(t)$ profiles with and without modulation and (b) the steering-wheel vibration $\theta_t(t)$: ——, results with a constant pressure $P(t \geqslant t_c) = P_{max}$; •••••, results with modulated $P(t)$

concluded that the lower pad contact stiffness and/or the higher bushing stiffness should effectively reduce the transient vibration. Although the bushing stiffness non-linearity is cited in the literature, its effect seems to be minimal (at least in the context of a simple model) since the operating range is relatively small and close to the origin. Finally, a new vibration control concept is proposed that modulates the actuation pressure based on an analytical solution of the disc angular displacement. The present analysis suggests that this concept is very promising in reducing the receiver vibration without sacrificing the brake performance. Further research should involve experimental validation of this concept as well as a more detailed non-linear analysis of the source (brake disc–caliper) dynamics. Also, high-order analysis will be needed to study more irregular thickness variations.

REFERENCES

1 **Jacobsson, H.** Aspects of disc brake judder, *Proc. IMechE, Part D: J. Automobile Engineering*, 2003, **217**(6), 419–430. DOI: 10.1243/095440703766518069.

2 **Jacobsson, H.** Analysis of brake judder by use of amplitude functions. SAE paper 1999-01-1779, 1999.

3 **Lee, K.** and **Dinwiddie, R. B.** Conditions of frictional contact in disk brake and their effects on brake judder. SAE paper 980598, 1998.

4 **Leslie, A. C.** Mathematical model of brake caliper to determine brake torque variation associated with disc thickness variation (DTV) input. SAE paper 2004-01-2777, 2004.

5 **Cho, H., Cho, C.,** and **Kim, C. B.** Thermal and mechanical performance analysis in accordance with disk stiffness changes in automotive disk brake. SAE paper 2007-01-3661, 2007.

6 **Kang, J.** and **Choi, S.** Brake dynamometer model predicting brake torque variation due to disc thickness variation. *Proc. IMechE, Part D: J. Automobile Engineering*, 2007, **221**(1), 49–55. DOI: 10.1243/09544070JAUTO91.

7 **Gassmann, S.** and **Engel, H. G.** Excitation and transfer mechanism of brake judder. SAE paper 931880, 1993.

8 **Kim, M. G., Jeong, H. I.,** and **Yoo, W. S.** Sensitivity analysis of chassis system to improve shimmy and brake judder vibration on steering wheel. SAE paper 960734, 1996.

9 **Abdelhamid, M. K.** Brake judder analysis using transfer functions. SAE paper 973018, 1997.

10 **Meyer, R.** Brake judder – analysis of the excitation and transmission mechanism within the coupled system brake, chassis and steering system. SAE paper 2005-01-3916, 2005.

11 **Singh, A.** and **Lukianov, G.** Simulation process to investigate suspension sensitivity to brake judder. SAE paper 2007-01-0590, 2007.

12 **de Vries, A.** and **Wagner, M.** The brake judder phenomenon. SAE paper 920554, 1992.

13 **Wu, M.** and **Shi, M.** Simulated and experimental study of hydraulic anti-lock braking system using sliding-mode PWM control. *Mechatronics*, 2003, **13**, 331–351.

14 **Duan, C.** and **Singh, R.** Influence of harmonically-varying normal load on steady state behavior of a 2DOF torsional system with dry friction. *J. Sound Vibr.*, 2006, **294**, 503–528.

15 **Duan, C.** and **Singh, R.** Forced vibrations of a torsional oscillator with Coulomb friction under a periodically-varying normal load. *J. Sound Vibr.*, 2009, **325**, 499–506.

APPENDIX

Notation

A	pressurized area
C	viscous damping term
D	disc thickness variation
I	moment of inertia
K	stiffness
m	mass
P	hydraulic pressure
r	radius
R	moment arm
t	time
T	torque
u	translational displacement
V	vehicle speed
θ	angular displacement
μ	friction coefficient
ω	angular speed

Subscripts

b	bushing
c	transition point
d	disc
eff	effective
max	maximum
p	pad
s	suspension
t	steering

Superscripts

$\dot{}$	$= \mathrm{d}(\ )/\mathrm{d}t$
$\ddot{}$	$= \mathrm{d}^2(\ )/\mathrm{d}t^2$